# Local Luminosity Function at 15$\mu m$ and Galaxy Evolution Seen by ISOCAM 15$\mu m$ Surveys

Cong Xu

Infrared Processing and Analysis Center, Jet Propulsion Laboratory, Caltech 100-22, Pasadena, CA 91125

Received Nov. 30, 1999; accepted ...

## ABSTRACT

A local luminosity function at $15\mu m$ is derived using the bivariate ($15\mu m$ vs. $60\mu m$ luminosities) method, based on the newly published ISOCAM LW3-band ($15\mu m$) survey of the very deep IRAS $60\mu m$ sample in the north ecliptic pole region (NEPR). New IRAS $60\mu m$ fluxes are obtained using the SCANPI/SUPERSCANPI software at the new ISOCAM positions of the sources in the sample. It is found to be in excellent agreement with the $15\mu m$ local luminosity function published by Xu et al (1998), which is derived from the *predicted* $15\mu m$ luminosities of a sample of IRAS $25\mu m$ selected galaxies. Model predictions of number counts and redshift distributions based on the local luminosity function and assumptions of its evolution with the redshift are calculated and compared with the data of ISOCAM $15\mu m$ surveys. Strong luminosity evolution on the order of $L \propto (1+z)^{4.5}$ is suggested in these comparisons, while pure density evolution can be ruled out with high confidence. The sharp peak at about 0.4mJy in the Euclidean normalized differential counts at $15\mu m$ can be explained by the effects of MIR broadband emission features, eliminating the need for any hypothesis for a 'new population'. It is found that the contribution from the population represented by ISOCAM $15\mu m$ sources can account for the entire IR/submm background, leaving little room for any missing 'new population' which can be significant energy sources of the IR/submm sky.

*Subject headings:* galaxies: luminosity function, mass function – galaxies: photometry – galaxies: starburst – galaxies: statistics – infrared: galaxies

## 1. Introduction

Our understanding of galaxy formation and evolution in the early epochs of the Universe has been vastly improved in the past a few years, thanks mainly to new deep surveys in a wide range of wavebands, ranging from the HST's WFPC (UV and optical) and NICMOS (NIR) surveys in the Northern and Southern Hubble Deep Fields (Williams et al. 1996; Williams et al. 1998; Thompson et al. 1999) to the SCUBA submm surveys (see Blain et al. 1999b for a review). In particular, several mid-infrared (MIR) and far-infrared (FIR) deep surveys (see Elbaz et al. 1998b, Puget & Lagache 1998 for reviews) were conducted using the Infrared Space Observatory (ISO) (Kessler et al. 1996) during its 29 months mission (Nov. 1995 – April. 1998). The new results from these surveys (Aussel et al. 1998; Puget et al. 1999; Dole et al. 1999) indicate significant improvements in sensitivity and accuracy over the earlier published results (Rowan-Robinson et al. 1997; Kawara et al. 1998). Strong cosmic evolution in the population of infrared-emitting galaxies is indicated in these results (Rowan-Robinson et al. 1997; Kawara et al. 1998; Aussel et al. 1998; Puget et al. 1999), consistent with the results of SCUBA surveys (Blain et al. 1999a) and with the scenario hinted by the newly discovered cosmic IR background (CIB) (Puget et al. 1996; Hauser et al. 1998; Dwek et al. 1998; Fixsen et al. 1998). These results challenge those from the UV/optical surveys (Madau et al. 1998; Pozzetti et al. 1998) in the sense that substantially more (i.e. a factor of 3 – 5) star formation in the earlier Universe with $z \gtrsim 2$ may be hinted in the IR/submm counts and in the CIB (see, e.g. Rowan-Robinson et al. 1997) compared to that derived from the UV/optical surveys (Madau et al. 1998; Pozzetti et al. 1998). The reason of this discrepancy is attributed to dust extinction which may hide much of the star formation in the early Universe from the UV/optical surveys (see Lonsdale 2000 for a review).

The best observed band in these ISO surveys is the ISOCAM LW3 ($15\mu$m) band, with 14 surveys covering a wide range of flux density from 0.05 mJy to 50 mJy (Elbaz et al. 1998b). Compared to the longer wavelength ISOPHOT surveys (e.g. $175\mu m$ FIRBACK survey, Puget et al. 1999), ISOCAM LW3 surveys have the advantage of using large detector arrays ($32 \times 32$ compared to the $2 \times 2$ array of the ISOPHOT-C200 camera) and having much better angular

resolution which allowed the surveys to go very deep ($\sim 0.1$ mJy compared to sensitivity limits of $175\mu m$ surveys of $\sim 100mJy$) before reaching the confusion limit. In addition to the indication of the significant cosmic evolution of IR galaxies, two other very interesting results are emerging from these MIR surveys:

1. The Euclidean normalized differential number counts of the $15\mu m$ band have a sharp peak at about 0.4 mJy (Elbaz et al. 1999) which, Elbaz et al. (1998a) claims, can only be explained by adding to the number count model a new population of objects which emerge (with increasing z) rapidly after $z \sim 0.4$ and start to dominate the counts below 1 mJy, but contribute negligibly in brighter flux range (Fig.10 of Elbaz et al. 1998a).

2. Subject to the substantial uncertainties in their IR SEDs, the integrated light of the galaxies detected in $15\mu m$ surveys may account for most the IR/submm background (Elbaz et al. 1999).

Taken at face values these results may have far-reaching impact on the studies of galaxy evolution, suggesting that the objects most responsible for the CIB, which are mostly missed by the UV/optical surveys, are already identified in the $15\mu m$ surveys and, perhaps more interestingly, they are from a new population not seen in the local Universe (i.e. not among the IRAS sources which in general have $z \lesssim 0.1$).

However, scrutiny on these interpretations of $15\mu m$ counts is needed because of the following two complications: (1) the effects of prominent emission features in the wavelength range of 3 – $13\mu m$ (Puget and Leger 1989) which can cause very significant K-corrections in MIR surveys (Xu et al. 1998); and (2) the lack of a local luminosity function (LLF) in the $15\mu m$ band which is needed for the quantitative determination of the evolution rate from the number counts (to date, the IRAS $12\mu m$ luminosity functions have been mostly used in the interpretation of the ISOCAM $15\mu m$ counts, resulting in large uncertainties due to the significant variations of the $f_{15\mu m}/f_{15\mu m}$ among galaxies; see Elbaz et al. 1999). Indeed, the source count model of Xu et al. (1998), which takes into account the effect of the MIR emission features, did predict the bumps and dips

in counts similar to what is seen in the $15\mu m$ surveys. Accordingly, Xu et al. (1998) made the warning that determinations of the evolution rate based on the slope of source counts will have to treat the effects of the MIR emission features carefully. Xu et al. (1998) also derived a LLF at $15\mu m$ from the *predicted* $15\mu m$ flux densities of a sample of 1406 IRAS $25\mu m$ selected galaxies based on a three component (cirrus/PDR, starburst, AGN) SED model.

Recently, Aussel et al. (1999b) published an ISOCAM $15\mu m$ survey of the very deep IRAS $60\mu m$ sample in the northern ecliptic pole region (NEPR) (Hacking and Houck 1987, hereafter HH87; Hacking 1987). In this paper, we will derive a new $15\mu m$ LLF based on results of this survey, and on the new IRAS SCANPI observations at $60\mu m$ of the same sources using the new ISOCAM positions. This is then compared to the LLF of Xu et al. (1998). With the confidence on the $15\mu m$ LLF gained from this new study we explore further, using the model of Xu et al. (1998), the quantitative interpretation of results of the ISOCAM deep surveys as published by Elbaz et al. (1999) and by Aussel et al. (1999a).

## 2. New $15\mu m$ LLF from NEPR Sample

### 2.1. New IRAS SCANPI observations at ISOCAM positions

The ISOCAM observations at $15\mu m$ for 94 out of 98 galaxies in the very deep IRAS $60\mu m$ sample in the NEPR (HH87) are described out by Aussel et al. (1999b). Altogether 106 sources were detected with signal to noise ratios $\geq 3$. Several IRAS sources correspond to multiple ISOCAM sources, given the much better angular resolution of ISOCAM ($\sim 10''$) compared to the IRAS resolution ($> 1'$). The mean position offset of the ISOCAM sources relative to IRAS positions (HH87) is $\sim 10''$.

New IRAS observations at $60\mu m$ using the IPAC software SCANPI were carried out at the positions of the 117 (11 having signal to noise ratio $< 3$) ISOCAM sources in the NEPR sample listed in the Table 3 of Aussel et al. (1999b), exploiting the IRAS survey database. This is to get a better corresponding $60\mu m$ flux density for each ISOCAM source, and also to bring

the IRAS flux densities obtained by HH87 to the newest IRAS standard (Moshir et al. 1992). For this task, three SCANPI queries were run and finished on Oct. 28, 1999, using the default settings of SCANPI[1]. Of the 117 sources, 99 are detected at $60\mu m$. For the 18 ISOCAM sources undetected by SCANPI, the interactive SUPERSCANPI has been run in attempts to increase the sensitivity when, in addition to the survey data, data from pointed observations (HH87; Gregorich et al. 1995) are also available. As in HH87 we include only pointed observations with 'deep-sky' macros in the SUPERSCANPI processing. Five additional detections were obtained through the SUPERSCANPI coadds. This leaves 13 ISOCAM sources undetected in the $60\mu m$ band, which have in general large offsets (<offset>$\sim 60''$) from the original IRAS positions. Of the 104 sources detected by SCANPI and SUPERSCANPI in the $60\mu m$ band, many (usually those corresponding to the same source in HH87 list) are confused together. The plots of SCANPI and SUPERSCANPI processing of these confused sources awere manually inspected to determine the best total flux densities of these confused sources, which are assigned to them jointly. A final list of 106 sources is given in Table 1, including the sources undetected by SCANPI/SUPERSCANPI, and the 4 sources for which Aussel et al. reported only upper limits at $15\mu m$. Redshifts are found for 68 of them from Ashby et al. (1996).

The SCANPI/SUPERSCANPI results are compared with the flux densities reported by HH87 and with those from the IRAS Faint Source Survey (FSS) (Moshir et al. 1992) for sources which observe the following criteria: (1) ISOCAM position within $20''$ of the IRAS position, (2) not confused with any other sources in the IRAS $60\mu m$ band, and (3) for FSS comparison, they have to be listed in the Faint Source Catelog (FSC) or in the Faint Source Reject File (FSR) in the IRAS database. Thirty sources are selected by the first two criteria, 27 of them also pass the criterion (3). It is found (Fig.1a and 1b) that the $60\mu m$ flux densities obtained in this paper are consistent with those listed in the FSC and FSR, but about 20% higher than those reported by HH87. Given that the FSC and FSR results represent the new standard of IRAS products,

---

[1]For details of SCANPI and SUPERSCANPI processing, see the webpage

*http : //www.ipac.caltech.edu/ipac/iras/scanpi_interp.html.*

it is likely that the lower flux densities of HH87 are due to some systematic biases in the early processing of IRAS data.

### 2.2. New $15\mu m$ LLF Derived from Bivariate $15\mu m/60\mu m$ LF

Exploiting the NEPR sample, a LLF at $15\mu m$ can be constructed using the so called 'bivariate method' (see, e.g., Xu et al. 1998), transferring the $60\mu m$ LLF of IRAS galaxies, which has been well studied in the literature (Soifer et al. 1987; Saunders et al. 1991; Yahil et al. 1992), to $15\mu m$ LLF utilizing the $L_{15\mu m}/L_{60\mu m}$ ratio v.s. $L_{60\mu m}$ relation. We include only the 64 sources in Table 1 which are detected in the $60\mu m$ band (including sources with upperlimits at $15\mu m$) and which have measured redshifts (Ashby et al. 1996).

There are several concerns with regarding to the sample:

- The sample is incomplete. In particular, the requirement of redshift availability excludes about one third of the sources in Table 1.
- Possible misidentification between the sources in the redshift survey of Ashby et al. (1996) and the sources in this work.
- Given the depth, the sample is not really local (many sources with $z > 0.1$), hence may be affected by galaxy evolution with increasing redshift.
- The redshift distribution of the sources shows strong clustering (Ashby et al. 1996).

Will these affect the bivariate $15\mu m/60\mu m$ luminosity function? The answer to this question depends on whether the $15\mu m$-to-$60\mu m$ color ratio is a sensitive function of the luminosity. This is because all the above potential problems with the sample are related to the reshift, and result in uncertainties in the luminosity distribution (the 'visibility function') but not in the $L_{15\mu m}/L_{60\mu m}$ ratio distribution. If the color ratio is insensitive to the luminosity, the conditional probability function $\Theta(L_{15\mu m}/L_{60\mu m}|L_{60\mu m})$ (cf. Eq(7) of Xu et al. 1998), which converts the $60\mu m$ LLF

to the $15\mu m$ LLF, will be rather constant and won't be affected significantly by uncertainties associated with the luminosity.

Indeed, as plotted in Fig.2, the $L_{15\mu m}/L_{60\mu m}$ ratios of sources in the NEPR sample appears to be rather insensitive to the luminosity. This result is similar to that of Soifer and Neugebauer (1991) who found that the $L_{25\mu m}/L_{60\mu m}$ ratio does not depend on the infrared luminosity. This may not be surprising given that the mechanisms of the $15\mu m$ emission and of the $25\mu m$ emission are nearly the same, namely due dominantly to the emission of small grains undergoing temperature fluctuations in normal galaxies such as the Milky Way, and to the warm dust emission associated with star formation regions in starburst galaxies such as M82 (Désert et al. 1990). This dualism in the radiation mechanism of the MIR continuum, at the wavelengths not contaminated by the MIR emission features, is the major reason for the lack of dependence of the two color ratios ($L_{15\mu m}/L_{60\mu m}$ and $L_{25\mu m}/L_{60\mu m}$) on luminosity. At the same time, the very cold $L_{25\mu m}/L_{60\mu m}$ ratios of ultraluminouse galaxies (ULIRGs), which are due mostly to extinction at $25\mu m$ (Xu and De Zotti 1989), also further weaken any statistical dependence of the $L_{25\mu m}/L_{60\mu m}$ ratio on the grain temperature, the latter is a strong function of the luminosity as demonstrated by the $L_{60\mu m}/L_{100\mu m}$ v.s. luminosity relation (Soifer and Neugebauer 1991).

The algorithm and the formulation used in this work are the same as presented in Section 3 of Xu et al. (1998)[2]. The $60\mu m$ LLF derived by Saunders et al. (1991) using the so-called 'non-parametric maximum-likelihood' method is taken, for which the effects of spatial galaxy density fluctuations, in particular the local over-density due to the local super cluster, are minimized (Saunders et al. 1991). In Table 2 the derived $15\mu m$ LLF is listed, with $L_{15\mu m}$ being defined by $\nu L_\nu$ at $15\mu m$ and bin width $\delta \log(L_{15\mu m}) = 0.4$. In Fig.3 this new $15\mu m$ LLF is compared to the $15\mu m$ LLF of Xu et al. (1998) which is derived from the *predicted* $15\mu m$ luminosities of a $25\mu m$ selected sample of IRAS galaxies. Excellent agreement, in particular near the knee of the LLF ($\sim 10^{9.5}$ $L_\odot$), is found between these two LLFs, which are derived from completely different data

[2]There was an error in Eq(14) of Xu et al. (1998), which should have been $Covar(F_{i-1}, F_i) = F_i \times Var(F_{i-1})/F_{i-1}$.

sets using very different approachs. This verifies that both LLFs are reliable within the limits of their uncertainties. On the other hand, the two LLFs are complementary to each other. While the new LLF is derived from *real* $15\mu m$ ISOCAM data obtained by Aussel et al. (1999b), the size of this data set (64 galaxies) is much smaller than the IRAS sample (1406 galaxies) used by Xu et al. (1998). Consequently, the new LLF does not extend as far as the LLF of Xu et al. (1998) beyond $L_*$, namely being truncated at $10^{11.3}$ $L_\odot$ and with the point at $10^{10.9}$ missing since there is no galaxy in that bin. It should be noted that both the $60\mu m$ LLF of Saunders et al. (1991) on which this work is based, and the $25\mu m$ LLF of Shupe et al. (1998) on which the $15\mu m$ LLF of Xu et al. (1998) is based, are derived using the maximum-likelihood method which minimizes the effect of density fluctuations. Also both the normalizations of the $60\mu m$ LLF of Saunders et al. (1991) and the $25\mu m$ LLF of Shupe et al. (1998) are carefully determined, which are transferred by the bivariate analyses to the $15\mu m$ LLFs of Xu et al. (1998) and of this work, respectively. The very good agreement between the points of the two $15\mu m$ LLFs near the knee (Fig.3) demonstrates that both normalizations are indeed reliable, eliminating a large uncertainty in the predction of the local $15\mu m$ counts (Elbaz et al. 1999). In what follows we will use the LLF of Xu et al. (1998) when $15\mu m$ LLF is needed.

## 3. Galaxy Evolution Indicated by ISOCAM $15\mu m$ Counts

In Fig.4 we reproduce the results of ISOCAM $15\mu m$ surveys presented in Elbaz et al. (1999). In addition, counts derived based on the *predicted* $15\mu m$ flux densities of sources in the IRAS $25\mu m$ selected sample of Xu et al. (1998) are plotted at the flux density levels $> 0.2$ Jy. Counts fainter than 0.2 Jy are not plotted since they drop dramatically, indicating the increasingly severe incompleteness, due to the fact that the sample is $25\mu m$ selected rather than $15\mu m$ selected. Note that at the bright end ($\geq 0.5$Jy) the normalized counts of these sources are significantly higher than the counts in the fainter flux density bins. This excess of counts is very likely due to the overdensity associated with the local supercluster (Lonsdale et al. 1990; Saunders et al. 1991).

As pointed out by Elbaz et al. (1999), the Euclidean normalized ISOCAM $15\mu m$ counts

have a narrow and prominent peak at about 0.4 mJy. There have been suggestions that this peak indicates a new population of infrared sources emerging after redshift $z \sim 0.4$ (Elbaz et al. 1998a). On the other hand Xu et al. (1998) argued that such a feature can be caused by the broad-band emission features often associated to the polycyclic aromatic hydrocarbon molecules (PAH features, see Puget and Leger 1989). However the model predictions published by Xu et al. (1998), specified by two galaxy evolution models including one pure luminosity evolution model with evolution rate as $L = L_0 \times (1+z)^3$ and one pure density evolution with $\rho = \rho_0 \times (1+z)^4$, calculated using the number counts model which takes into account the effects of these emission features, underestimated the counts when compared with the ISOCAM data (Elbaz et al. 1998a). This suggests that the evolution endured by the ISOCAM sources is stronger than that assumed by Xu et al. (1998) which is based on previous studies of IRAS counts (Lonsdale et al. 1990; Saunders et al. 1991; Pearson and Rowan-Robinson 1996).

Here we present new model predictions using the same number count model of Xu et al. (1998), but with stronger evolution rates, and compare them with the ISOCAM $15\mu m$ data. We have assumed that galaxy formation starts at z=5 (the counts are not sensitive to this parameter). The cosmology adopted in the models plotted in Fig.4 is specified by $\Omega_m = 0.3$ and $\Omega_\Lambda = 0.7$, which is suggested by recent observations of type I supernovae in distant galaxies (Garnavich et al. 1998). Models with $\Omega_m = 1$ $\Omega_\Lambda = 0$ and with $\Omega_m = 0.3$ $\Omega_\Lambda = 0$ were also calculated, but not plotted here. The results from $\Omega_m = 0.3$ $\Omega_\Lambda = 0$ cosmology are very close to the results presented in Fig.4, while the results from the $\Omega_m = 1$ $\Omega_\Lambda = 0$ model fit the data slightly less well.

The solid line represents the pure luminosity evolution model with L$\propto (1+z)^{4.5}$ and with a turnover at $z = 1.5$ beyond which the evolution turns flat (i.e. L=constant for $z \geq 1.5$). The short-dashed line gives the counts predicted by another pure luminosity evolution model with L$\propto (1+z)^{4.8}$ and with a turnover at smaller redshift: z=1 (i.e. L=constant for $z \geq 1$). Finally the long-dashed line is the prediction for counts by a pure luminosity evolution model without any turnover, and with an evolution rate of L$\propto (1+z)^{4.3}$. Among the three luminosity evolution models, the one with turnover at z=1.5 (the solid curve) gives the best fit, closely reproducting

the overall shape and the level of the observed counts. The model with a turnover redshift z=1 predicts a peak too flat compared to the data. This is because, in the framework of Xu et al. (1998) model, the broadband MIR features in the wavelength range 6 - 8.5$\mu m$, which are redshifted into the ISOCAM LW3 bandpass when z=1±0.2, are largely responsible for the narrow peak of the counts in Fig.4. When the turnover occurs at z=1, a significant number of sources in the redshift range of z=1 - 1.2 are dropped compared to the models without turnover or with the turnover at 1.5, resulting in a less prominent peak. The model without turnover (the long-dashed line) predicts a peak at $f_{15\mu m} \sim$ 0.2mJy instead of 0.4mJy as shown by the data.

The dotted line shows the prediction by a density evolution model with comoving density $\rho \propto (1+z)^{7.5}$ until z=1.5, turning flat afterwards (i.e. $\rho$=constant when $z \geq 1.5$). This model gives reasonable fit to data points brighter than $f_{15\mu m} \sim$ 0.2mJy. However in the fainter flux levels, instead of turning down, the model prediction keeps rising in the plot until $f_{15\mu m}$ reaches as low as $\sim$ 0.04mJy. This is very different from the trend shown by the data. The reason for the difference between the density evolution model and the luminosity evolution models is that for a given redshift, say z=1 which allows the 6 - 8.5$\mu m$ emission features to be included in the LW3 bandpass, galaxies are much fainter in pure density evolution models compared to those in pure luminosity evolution models, therefore the bump caused by the K-correction due to the MIR emission features occurs in much fainter flux density levels (see Xu et al. 1998 for a more detailed discussion).

Strong constraints on galaxy evolution can be obtained when the redshift information of a flux-limited sample is available. Aussel et al. (1999a) found in the literature 29 redshifts for 49 sources in the main source list of the ISOCAM HDF (North) survey. In Fig.5 the histogram of the redshifts of 17 of these sources with $f_{15\mu m} \geq$ 0.1mJy is compared to the model predictions by the three models presented in Fig.4. A sky coverage of 5 acrmin$^2$ (Aussel et al 1999a) and a correction factor of 2 for the incompleteness are assumed in these calculations. All three luminosity evolution models give reasonably good fits to the data in the bins of $z < 1$, and over-predicts counts in bins of $z > 1$. In particular, both the model with turnover at z=1.5 and the model without turnover

predict some sources (6 by the former and 14 by the latter) with z> 1.4 while none is found in the data. For the model with turnover at z=1.5, the best fitting model in Fig.4, the missing of sources at $z > 1.4$ could be due to small number statistics or to the incompleteness of the data at high redshifts. This highlights the demand for larger and more complete redshift sample for ISO sources. In fact, when redshifts for a large (a few hundred) and complete flux limited sample are available, luminosity functions of ISO sources can be calculated for different redshift epochs which will give the most direct information about the evolution of these sources.

The reasonably good fits to both the source counts (Fig.4) and the redshift distribution (Fig.5) by the three luminosity evolution models (in particular the model of L$\propto (1+z)^{4.5}$ with a turnover at $z = 1.5$) demonstrate that indeed the narrow peak of the ISOCAM $15\mu m$ counts can be well explained by the effect of broadband MIR emission features which is the essential element of the model of Xu et al. (1998), and there is no need to invoke a 'new population'. At the same time, the evolution rate implied by the model fit is much stronger than those given by previous studies on IRAS sources (L$\propto (1+z)^3$, Pearson and Rowan-Robinson 1996; Lonsdale et al. 1990), but is consistent with what is found in the UV and optical deep surveys (L$\propto (1+z)^{3.95\pm0.75}$, Lilly et al. 1996). Analyzing multiband data from IRAS, ISO, SCUBA and COBE, Blain et al. (1999a) also obtained a relatively high evolution rate ((L$\propto (1+z)^{3.8\pm0.2}$). Given the lack of dependence of the $L_{15\mu m}/L_{60\mu m}$ ratio on the luminosity, one expects that the evolution rates of the $L_{15\mu m}$ and of the $L_{60\mu m}$ should be similar. In Fig.6 we compare the predicted counts at $60\mu m$ by a luminosity evolution model assuming $L_{60\mu m} \propto (1+z)^{4.5}$ which turns flat ($L_{60\mu m}$ =constant) at $z = 1.5$, with IRAS data. The large filled circles are the counts from this work (new NEPR sample), which are about 30% (i.e. $\sim$ 0.12 dex) higher than those of HH87 (crosses). This discrepancy can be fully explained by the fact that the $60\mu m$ fluxes obtained by the new SCANPI/SUPERSCANPI processings are about 20% higher than those of HH87 (Fig.1a), given that the Euclidean normalized differential counts scale with the flux to the 1.5 power. At the same time, the model predictions (solid line) indeed reproduce the trend and the level of those more recent IRAS counts (Bertin et al. 1997; Gregorich et al. 1995; Saunders et al. 1991; Lonsdale et al. 1990; Rowan-Robinson et al. 1990) quite well.

Pure density evolution, which gives poor fit to the number counts, can be ruled out with high confidence. Given that any density evolution will push the peak in the number counts to fainter flux levels than shown by the data, it is quite certain that, as far as choice between density and luminosity evolution is concerned, the luminosity evolution is the dominant drive in the cause of the high number counts. This conclusion is in agreement with that of Blain et al. (1999a) which is obtained from a completely different argument, namely that a pure density evolution model which can fit the IR/submm counts will produce too much IR/submm background.

Our results show that the narrow peak of the ISOCAM $15\mu m$ counts at about 0.4 mJy may not be used as an evidence for a 'new popultion' of faint MIR sources. On the other hand, a luminosity evolution in the luminosity function of infrared galaxies, as suggested by our best fitting model, does not necessarily mean that it is the same galaxies what we are seeing in the local Universe that are shining tens or even hundreds times brighter in the early epochs of the Universe. Indeed, the preliminary results of optical identifications of ISOCAM LW3 sources indicate that beyond $z \sim 0.7$ most of them are interacting galaxies (Aussel et al. 1999a; Elbaz et al. 1999), while the local MIR selected extragalactic sources are mostly single late type galaxies similar to the Milky Way (Rush et al. 1993). Given the high incompleteness of redshift data, at this stage the major constraint on the evolution of ISOCAM sources is from the counts, which is mostly determined by how the luminosity function evolves around $L_*$ (the luminosity distribution of sources in a given $f_{15\mu m}$ bin peaks strongly around $L_*$). Therefore, without any extrapolation, what we know now is that whatever the population is for IR sources at redshift $z \sim 1$, its comoving density is about the same as the IR galaxies in the local Universe, while the characteristic $15\mu m$ luminosity of the faint sub-mJy sources is about 20 times the $L_*$ of local IR galaxies, namely at $L_* \sim 10^{11}$ $L_\odot$ level. If these sources are indeed similar to the local gas-rich spiral-spiral galaxy pair systems, which dominate the bright end ($L_{fir} > 2 \times 10^{11} L_\odot$) of IRAS luminosity function (Xu and Sulentic 1991), the implied density enhencement of these sources at $z \sim 1$ compared to their density in the local Universe is more than an order of magnitude. Although the population of these interacting galaxies is not really 'new' (i.e. they are already important contributors of MIR counts in the local Universe), it is quite possible that this population may evolve much faster than

normal late-type galaxies, and even than AGNs. For the sake of simplicity, we have treated all IR galaxies as a single population in our model and have not considered any 'differential evolution' (i.e. different evolution rates for galaxies with different luminosities). When more constraints on the nature of $15\mu m$ sources are available from future follow-up observations, a model treating the evolution of different galaxy populations differently (e.g. separating interacting galaxies from single galaxies and AGNs), such as the model by Franceschini et al. (1994), will be more appropriate.

Our results also suggest that the MIR emission features are present in the SEDs of galaxies with redshifts up to $z \sim 1$. Whether this is still true for galaxies with even larger redshifts will be found out by the future SIRTF mission (Cruikshank and Werner 1997). If so, these features will facilitate a powerful new method of obtaining redshifts in infrared for optically faint, heavily extinguished galaxies.

As for the question whether galaxy evolution has a turnover at z=1–2, our results are not conclusive, though a positive answer is favoured by the model fits (Fig.4). Given the significant effect of the MIR emission features, which happens to affect the $15\mu m$ counts at redshift just below z=1.5, the turnover favoured by our model may well be a false signal. Deep surveys at longer wavelengths (e.g. at $25\mu m$ and $70\mu m$ using SIRTF/MIPS detector arrays) where the MIR features will be redshifted into the bandpass at larger z, are certainly desirable for the determination of the evolution of IR galaxies beyond z=1.5 (Xu et al. 1998).

How much is the contribution from these sources to the IR/sub-mm Cosmic background radiation? To answer this question, a Monte Carlo simulation based on the source count model of Xu et al. (1998) was carried out, assuming the galaxy evolution model that gives the best fit of the data in Fig.4 (namely L$\propto (1+z)^{4.5}$ with a turnover at $z = 1.5$). Sources with certain $L_{15\mu m}$ and z are generated according to predictions of the number count model, and IR SEDs taken from the SED sample of 1406 galaxies in Xu et al. (1998) are assigned to these sources in accordance with their rest frame $L_{15\mu m}$. It should be noted that the SEDs modeled by Xu et al. (1998) stop at $120\mu m$. In order to estimate the contribution from MIR galaxies to the IR background

radiation at longer wavelengths, we have assumed that the IR emission at $\lambda > 120\mu m$ of all sources generated in the simulation have the same spectrum specified by a modified blackbody with $T = 40$K and the emissivity index of $\beta = 1.5$ (Blain et al. 1999). In reality, this submm SED may only apply to the luminous IR starburst galaxies (LIRGs) while the SEDs of less active galaxies are likely to be much colder (Eales et al. 1999). However, since the largest contribution to the submm background is from LIRGs (Blain et al. 1999), we neglect this complication here.

For any given wavelength, all the fluxes from these simulated sources are summed up, resulting in the predicted contribution of the population of $15\mu m$ sources at the wavelength in question. Again we assume that the galaxy formation starts at z=5. In Fig.7, this prediction (the solid curve) is plotted against several measurements/upper-limits of the IR/submm background. The upperlimits are all from the studies of TeV gamma-ray sources (Dwek & Slavin 1994; Stanev & Franceschini 1998). The filled circles with error bars are COBE/DIRBE results taken from Lagache et al. (1998), and the large crosses are from SCUBA results (Blain et al. 1999). The two dashed curves outline the range of the submm IR background detected by COBE/FIRAS (Fixen et al. 1998). According to our results, the contribution of the MIR galaxies to the background between 10–30$\mu m$ is at the 4 nW/m$^2$/sr level, compared to the results reported by Elbaz et al. (1999) that the $15\mu m$ background due to sources brighter than 50$\mu$Jy is 3.3 nW/m$^2$/sr. Note that this already meets the upperlimits obtained by Stanev and Franceschini (1998) from the analysis of TeV emission of Mrk501. At longer wavelengths, predicted contribution to the background emission agrees very well at DIRBE points, and slightly above the upper-boundary of the measured submm background. Compared to the results of previous calculations on the cosmic IR background using 'backward evolution' models (Hacking and Soifer 1991; Beichman and Helou 1991; Malkan and Stecker 1998), the category this work belongs to, our result is about a factor of 2 higher because the evolution rate hinted by ISOCAM $15\mu m$ surveys is significantly stronger than those used in the previous works. Our result is in agreement with Elbaz et al (1999), who found that the ISOCAM $15\mu m$ sources may be able to account for the majority of the IR/submm background. Taken at face value, the result in Fig.7 indicates that nearly all of the sources contributing significantly to the IR/submm background are already present in the population of

$15\mu m$ sources detected by ISO, and very little room is left for any missing 'new population' which can be significant energy sources of the IR/submm sky.

The author is indebted to Gianfranco De Zotti, who not only suggested this project, but also provided stimulating comments on an earlier version of this paper. He also thanks Herve Aussel for informative and constructive discussions. Diane Engler, Iffat Khan, Joe Mazzarella and Steve Lord are thanked for helping to obtain and interpret the SCANPI/SUPERSCANPI results. David Gregorich and Perry Hacking are thanked for providing information on IRAS pointed observations in NEPR. Constructive comments on the manuscript from Carol Lonsdale and David Shupe, and from an anonymous referee are acknowledged. Part of the work is supported by NASA grant for ISO Data Analysis. This research has made use of the NASA/IPAC Extragalactic Database (NED) which is operated by the Jet Propulsion Laboratory, California Institute of Technology, under contract with the National Aeronautics and Space Administration. The author was supported by the Jet Propulsion Laboratory, California Institute of Technology, under contract with NASA.

## REFERENCES

Ashby, M.L.N., Hacking, P.B., Houch, J.R., Soifer, B.T., Weisstein, E.W. 1996, ApJ, 456, 428.

Aussel, H., Cesarsky, C.J., Elbaz, D., Starck, J.L. 1999a, A&A, 342, 313

Aussel, H., Coia, D., Mazzei, P., De Zotti, G., Franceschini, A. 1999b, A&A, in press.

Beichman, C.A., Helou, G. 1991, ApJ, 370, L1

Blain, A.W., Smail, I., Ivison, R.J., Kneib, J.-P. 1999a, MNRAS, 302, 632.

Blain, A.W., Smail, I., Ivison, R.J., Kneib, J.-P. 1999b, astro-ph/9908111.

Cruikshank, D.P. and Werner, M.W. 1997, in "Planets Beyond the Solar System", ed. D.R. Soderblom, Ast. Soc. Pacific Conference Series, 119, 223.

Désert, F.-X., Boulanger, F., Puget, J.-L. 1990, A&A, 237, 215.

Dole, H., Lagache, G., Puget, J-L., et al. 1999, astro-ph/9902122

Dwek, E., Arendt, R.G., Hauser, M.G., et al. 1998, ApJ, 508, 106.

Dwek, E., Slavin, J. 1994, ApJ, 436, 696.

Eales, S.A., Lilly, S.J., Gear, W.K., et al. 1999, ApJ, 515, 518.

Elbaz, D., Aussel, H., Baker, A.C., et al. 1998a, astro-ph/9807209.

Elbaz, D., Aussel, H., Cesarsky, C.J., et al. 1998b, in *The Universe as Seen by ISO*, eds. P. Cox & M.F. Kessler, p999.

Elbaz, D., Cesarsky, C.J., Fadda, D. , et al. 1999, A&A, 351, L37.

Fixen, D.J., Dwek, E., Mather, J.C., Bennett, C.L., Shafer, R.A. 1998, ApJ, 508, 123.

Franceschini, A., Mazzei, P., De Zotti, G., Danese, G. 1994, ApJ, 427, 140.

Garnavich, P.M., Jha, S., Challis, P. et al. 1998, ApJ, 509, 74.

Gregorich, D.T., Neugebauer, G., Soifer, B.T., Gunn, J.E., Herter, T.L. 1995, AJ, 110,259.

Hacking, P. 1987, Ph.D. thesis.

Hacking, P., Houck, J.R. 1987, ApJS, 63, 311 (HH87).

Hacking, P.B., Soifer, B.T. 1991, ApJ, 367, L49.

Hauser, M. G., Arendt, R. G., Kelsall, T., et al. 1998, ApJ, 508, 25.

Kawara, K., Sato, Y., Matsuhara, H., et al. 1998, A&A, 336, L9.

Kessler, M.F., Steinz, J.A., Anderegg, M.E. et al. 1996, A&A, **315**, L27.

Lagache, G., Abergel, A., Boulanger, F., Puget, J.-L. Puget 1998, A&A, 333, 709.

Lilly, S.J., Le Févre, O., Hammer, F., Crampton, D. 1996, ApJ, 460, L1.

Lonsdale, C.J. 1999, in *Astrophysics with Infrared Surveys: A Prelude to SIRTF*, ASPC Series **177**, eds. M.D. Bicay, C.A. Beichman, R.M. Cutri, and B.F. Madore, p24.

Lonsdale, C.J., Hacking, P.B., Conrow, T.B., Rowan-Robinson, M. 1990, ApJ, 358, 20.

Madau, P., Pozzetti, L., Dickinson, M. 1998, ApJ, 498, 106.

Malkan, M.A., Stecker, F.W. 1998, ApJ, 496, 13.

Moshir M., et al. 1992, IRAS Faint Source Catalog Explanatory Supplement, Version 2.

Pearson, G., and Rowan-Robinson, M. 1996, MNRAS, 283, 174.

Pozzetti, L., Madau, P., Zamorani, G., Ferguson, H.C., Bruzual, G. 1998, MNRAS, 298, 1133.

Puget, J-L., Albergel, A., Boulanger, F., et al. A&A, 308, L5.

Puget, J-L., Lagache, G. 1998, in *The Universe as Seen by ISO*, eds. P. Cox & M.F. Kessler, p1007.

Puget, J-L., Lagache, G., Clements, D.L, et al. 1999, A&A, 345, 29.

Puget, J.L., and Léger, A.,1989, ARA&A, 27, 161.

Rush, B., Malkan, M.A., Spinoglio, L. 1993, ApJS, 89, 1.

Rowan-Robinson, M., Hughes, J., Vedi, K., Walker, D.W. 1990, MNRAS, 246, 473.

Rowan-Robinson, M., Mann, R.G., Oliver, S.J., et al. 1997, MNRAS, 289, 490.

Shupe, D.L., Fan, F., Hacking, P.B., Huchra, J.P. 1998, ApJ, 501, 597.

Saunders, W., Rowan-Robinson, M., Lawrence, A. et al. 1991, MNRAS, 242, 318.

Soifer, B.T., Sanders, D.B., Madore, B.F., Neugebauer, G. et al. 1987, ApJ, 320, 238.

Soifer, B.T., Neugebauer, G. et al. 1991, AJ, 101, 354.

Stanev, T., Franceschini, A. 1998, ApJ, 494, L159.

Thompson, R.I., Storrie-Lombardi, L.J., Weymann, R.J., Rieke, M.J., Schneider, G., Stobie, E., Lytle, D. 1999, AJ, 117, 17.

Williams, R.E. et al. 1996, AJ, 112, 1335.

Williams, R.E. et al. 1998, BAAS, 193. 7501

Xu, C., De Zotti, G. 1989, A&A, 225, 12.

Xu, C., Hacking, P.B., Fan, F., Shupe, D.L., Lonsdale, C.J., Lu, N.Y., Helou, G.X., 1998, ApJ, 508, 576.

Xu, C., Sulentic, J.W. 1991, ApJ, 374, 407.

Yahil, A., Strauss, M., Davis, M., Huchra, J.P. 1992, ApJ, 372, 380.

---

This manuscript was prepared with the AAS LaTeX macros v4.0.

Table 1. New $f_{60\mu m}$ for the NEPR sample

| I.D.[1] | $f_{60\mu m}$[2] | error[3] | $f^{HH}_{60\mu m}$[4] | offset [5] | redshift[6] |
|---|---|---|---|---|---|
| (HH87) | (mJy) | (mJy) | (mJy) | (″) | |
| 3-01 | | 27 | 83 | 81.5 | 0.116 |
| 3-02 | 80 | 16 | 85 | 104.8 | |
| 3-03 | 140 | 17 | 100 | 6.6 | 0.089 |
| 3-04 | 250 | 20 | 190 | 7.1 | 0.121 |
| 3-05 | 85 | 18 | 100 | 11.3 | 0.0408 |
| 3-07 | 110 | 14 | 78 | 7.4 | 0.0417 |
| 3-08 | 220 | 13 | 170 | 1.6 | 0.052 |
| 3-09 | | 25 | 73 | 17.6 | 0.0255 |
| 3-10 | 330 | 21 | 260 | 8.3 | |
| 3-11 | 170 | 22 | 110 | 7.4 | 0.0250 |
| 3-12 | 150 | 17 | 130 | 23.4 | 0.0766 |
| 3-13 | 64 | 25 | 66 | 29.2 | 0.201 |
| 3-14 | 130 | 12 | 99 | 13.5 | 0.0421 |
| 3-15 | 130 | 23 | 110 | 14.3 | 0.0780 |
| 3-16 | 90 | 14 | 92 | 20.9 | 0.117 |
| 3-17a | | 16 | | 42.1 | |
| 3-17b | 60 | 14 | 63 | 12.8 | 0.0704 |
| 3-18 | 140 | 25 | 82 | 56.3 | 0.229 |
| 3-19abc | 130 | 17 | 74 | 30.6 | 0.0872 |
| 3-20ab | 103 | 17 | 62 | 52.3 | 0.0735 |
| 3-21 | 60 | 10 | 64 | 17.8 | 0.0522 |

Table 1—Continued

| I.D.[1] | $f_{60\mu m}$[2] | error[3] | $f_{60\mu m}^{HH}$[4] | offset [5] | redshift[6] |
|---|---|---|---|---|---|
| (HH87) | (mJy) | (mJy) | (mJy) | (″) | |
| 3-23 | 90 | 22 | 87 | 15.0 | 0.0878 |
| 3-24 | 90 | 13 | 74 | 9.1 | |
| 3-25 | 100 | 20 | 77 | 20.7 | 0.0853 |
| 3-26abcd | 150 | 10 | 140 | 21.3 | 0.089 |
| 3-27a | 110 | 12 | 87 | 26.1 | 0.0873 |
| 3-27b | 70 | 14 | | 55.6 | 0.0873 |
| 3-28 | 80 | 16 | 63 | 21.4 | 0.0253 |
| 3-29 | 50 | 14 | 57 | 24.3 | |
| 3-30 | 70 | 21 | 72 | 41.0 | 0.2540 |
| 3-31 | 170 | 12 | 190 | 5.8 | |
| 3-32a | 90 | 21 | 89 | 43.6 | 0.0375 |
| 3-32b | 30 | 13 | | 95.8 | 0.0375 |
| 3-33a | 70 | 12 | 56 | 24.0 | 0.1440 |
| 3-33b | | 12 | | 72.3 | |
| 3-34 | 100 | 14 | 89 | 9.0 | 0.0373 |
| 3-35 | 70 | 14 | 70 | 31.5 | 0.195 |
| 3-36a | | 71 | 66 | 8.2 | 0.119 |
| 3-36b | | 72 | | 69.9 | |
| 3-37 | 480 | 16 | 510 | 2.0 | |
| 3-38ab | 80 | 10 | 54 | 56.2 | |
| 3-39 | 80 | 26 | 57 | 14.2 | |

Table 1—Continued

| I.D.[1] | $f_{60\mu m}$[2] | error[3] | $f_{60\mu m}^{HH}$[4] | offset [5] | redshift[6] |
|---|---|---|---|---|---|
| (HH87) | (mJy) | (mJy) | (mJy) | (″) | |
| 3-40ab | 110 | 26 | 98 | 27.7 | 0.0887 |
| 3-41 | 100 | 19 | 100 | 15.2 | |
| 3-42 | 50 | 16 | 60 | 39.1 | 0.1150 |
| 3-43 | 140 | 16 | 150 | 18.6 | 0.026 |
| 3-44 | 080 | 17 | 54 | 24.4 | |
| 3-45 | 160 | 18 | 140 | 6.7 | 0.0789 |
| 3-46 | 80 | 15 | 71 | 2.9 | 0.0360 |
| 3-47 | 160 | 22 | 110 | 28.9 | 0.0867 |
| 3-48 | 160 | 17 | 140 | 23.6 | 0.0259 |
| 3-49 | 50 | 16 | 54 | 14.6 | |
| 3-50 | 100 | 26 | 89 | 6.7 | 0.0876 |
| 3-51a | 160 | 11 | 130 | 9.0 | |
| 3-51b | | 18 | | 96.2 | |
| 3-53 | 400 | 29 | 330 | 3.2 | |
| 3-54 | 80 | 16 | 74 | 14.6 | 0.0799 |
| 3-55 | 70 | 22 | 54 | 15.6 | |
| 3-56 | 110 | 19 | 110 | 10.7 | 0.0881 |
| 3-57 | 230 | 11 | 220 | 11.3 | |
| 3-58 | 80 | 13 | 50 | 14.7 | |
| 3-59 | 70 | 12 | 57 | 9.1 | |
| 3-61 | 160 | 15 | 150 | 6.0 | |

Table 1—Continued

| I.D.[1] | $f_{60\mu m}$[2] | error[3] | $f^{HH}_{60\mu m}$[4] | offset [5] | redshift[6] |
|---|---|---|---|---|---|
| (HH87) | (mJy) | (mJy) | (mJy) | (″) | |
| 3-62 | 110 | 20 | 83 | 12.0 | 0.0271 |
| 3-63a | 210 | 28 | 210 | 6.3 | 0.1180 |
| 3-63b | | 13 | | 104.3 | |
| 3-64 | 560 | 20 | 540 | 3.6 | |
| 3-65 | 110 | 11 | 120 | 18.7 | 0.173 |
| 3-66 | 96 | 8 | 89 | 10.7 | 0.0535 |
| 3-67ab | 110 | 11 | 97 | 23.5 | 0.0399 |
| 3-68 | 50 | 21 | 51 | 35.6 | |
| 3-69 | 50 | 20 | 61 | 15.2 | 0.104 |
| 3-70 | 140 | 10 | 100 | 8.4 | 0.197 |
| 3-71 | 80 | 13 | 72 | 3.1 | 0.0517 |
| 3-72 | 80 | 30 | 57 | 75.4 | |
| 3-73 | 230 | 13 | 250 | 13.6 | |
| 3-74 | 150 | 8 | 160 | 14.9 | 0.026 |
| 3-75 | | 19 | 65 | 23.6 | 0.0583 |
| 3-76 | 80 | 16 | 61 | 20.7 | 0.0800 |
| 3-77 | 100 | 16 | 120 | 57.1 | 0.0871 |
| 3-78a | | 12 | | 68.1 | |
| 3-78bc | 90 | 23 | 69 | 13.1 | 0.0774 |
| 3-79ab | 300 | 11 | 230 | 19.6 | |
| 3-79c | | 10 | | 110.7 | |

Table 1—Continued

| I.D.[1] | $f_{60\mu m}$[2] | error[3] | $f^{HH}_{60\mu m}$[4] | offset [5] | redshift[6] |
|---|---|---|---|---|---|
| (HH87) | (mJy) | (mJy) | (mJy) | (″) | |
| 3-80ab | 330 | 20 | 290 | 13.7 | |
| 3-81ab | 130 | 14 | 110 | 23.4 | 0.0268 |
| 3-82 | 220 | 13 | 200 | 6.1 | 0.0551 |
| 3-83 | 100 | 14 | 89 | 15.7 | 0.107 |
| 3-84 | 160 | 11 | 160 | 5.8 | 0.086 |
| 3-85 | 100 | 9 | 69 | 19.3 | 0.151 |
| 3-86 | 70 | 16 | 73 | 31.2 | |
| 3-88a | 100 | 17 | 74 | 29.0 | 0.519 |
| 3-88b | | 17 | | 86.9 | |
| 3-89 | 90 | 16 | 69 | 56.5 | 0.029 |
| 3-90 | 100 | 9 | 65 | 8.6 | 0.0720 |
| 3-91 | 80 | 11 | 58 | 15.2 | |
| 3-92abc | 90 | 19 | 75 | 56.9 | 0.0880 |
| 3-93 | 140 | 19 | 99 | 23.0 | 0.0690 |
| 3-94a | 130 | 16 | 98 | 3.7 | 0.0502 |
| 3-94b | | 20 | | 89.3 | |
| 3-96 | 190 | 18 | 150 | 5.8 | 0.0321 |
| 2-16 | 40 | 13 | 38 | 9.5 | |
| 3-06 | | | 62 | | 0.0754 |
| 3-22 | | | 88 | | |
| 3-87 | | | 55 | | |

Table 1—Continued

| I.D.[1] | $f_{60\mu m}$[2] | error[3] | $f^{HH}_{60\mu m}$[4] | offset [5] | redshift[6] |
|---|---|---|---|---|---|
| (HH87) | (mJy) | (mJy) | (mJy) | (″) | |
| 3-95 | | | 78 | | 0.187 |

[1]These are the same sources as listed in Table 3 of Aussel et al. (1999b). Sources confused with each other in $60\mu m$ band are grouped together and enter as single entries.

[2]$60\mu m$ flux density obtained in this work. For undetected sources the entry is blank.

[3]The one-$\sigma$ error of $f_{60\mu m}$.

[4]$60\mu m$ flux density taken from HH87. When more than one source are corresponding to a single HH87 source, the flux density is assigned to the one with the least offset.

[5]Offset of the $15\mu m$ source from the HH87 source, taken from Aussel et al. (1999b). When more than one $15\mu m$ source are corresponding to a single source here (confused sources), the smallest offset is taken.

[6]Redshift taken from Ashby et al. (1996).

Table 2. $15\mu m$ Local Luminosity Function (LLF) from NEPR sample

| $\log(\nu L_\nu(15\mu m)/L_\odot)$ | $\log(\phi/(\mathrm{Mpc}^{-3}\mathrm{mag}^{-1}))$ | $1\ \sigma$ error |
|---|---|---|
| 8.1 | -3.70 | -3.71 |
| 8.5 | -2.42 | -2.78 |
| 8.9 | -2.68 | -3.40 |
| 9.3 | -3.09 | -3.56 |
| 9.7 | -3.47 | -4.21 |
| 10.1 | -4.11 | -4.43 |
| 10.5 | -5.08 | -5.64 |
| 11.3 | -7.49 | -7.49 |

Fig. 1.— Comparisons between $f_{60\mu m}$ from this work (new SCANPI/SUPERSCANPI reductions) and from HH87 (Fig.1a), and from FSS (Fig.1b).

Fig. 2.— NEPR sources (64) used in the bivariate analysis: $L_{15\mu m}/L_{60\mu m}$ ratio versus $15\mu m$ luminosity.

Fig. 3.— $15\mu m$ local differential luminosity function.

Fig. 4.— Euclidean normalized $15\mu m$ differential counts: model predictions compared to the observations. The observational data are taken from Elbaz et al. (1999). Data points (same as in Elbaz et al. 1999): A2390 (stars); ISOHDF-North (open circles), ISOHDF-South (filled circles), Marano FIRBACK Ultra-Deep (open squares), Marano Ultra-Deep (exes), Marano FIRBACK Deep (stars), Lockman Deep (open triangles), Lockman Shallow (filled triangles). At the bright end ($> 0.2Jy$) plotted (filled squares) are the counts derived based on the *predicted* $15\mu m$ flux densities of the sources in the sample of Xu et al. (1998).

Fig. 5.— Redshift distribution of ISOCAM $15\mu m$ sources in the field of ISOHDF-North (Aussel et al. 1999a): model predictions compared to the observational data.

Fig. 6.— Euclidean normalized differential counts of IRAS $60\mu m$ band: model predictions compared to the observations. Data points: new NEPR (this work) (large filled circles); HH87 (exes); Gregorich et al. 1995 (open stars); Bertin et al. 1997 (open circles); Lonsdale et al. 1990 (filled squares); Saunders et al. 1991 (filled squares), Rowan-Robinson et al. 1990 (open squares). Model: $L_{60\mu m} \propto (1+z)^{4.5}$ when $z \leq 1.5$, $L_{60\mu m}$ =constant when $z > 1.5$ (solid line).

Fig. 7.— Cosmic IR/submm background: model predictions compared to the observational data. Symbols: Model prediction ($z \leq 1.5$: L$\propto (1+z)^{4.5}$; $1.5 < z \leq 5$: L=constant) — solid curve; COBE/DIRBE results (Lagache et al. 1998) — large filled circles with error bars; SCUBA results (Blain et al. 1999) — large crosses; the range of COBE/FIRAS results (Fixen et al. 1998) — two dashed curves; upperlimits from TeV gamma-ray radiation of Mrk403 and Mrk501 (Dwek & Slavin 1994; Stanev & Franceschini 1998) — diamonds and exes with upperlimits.

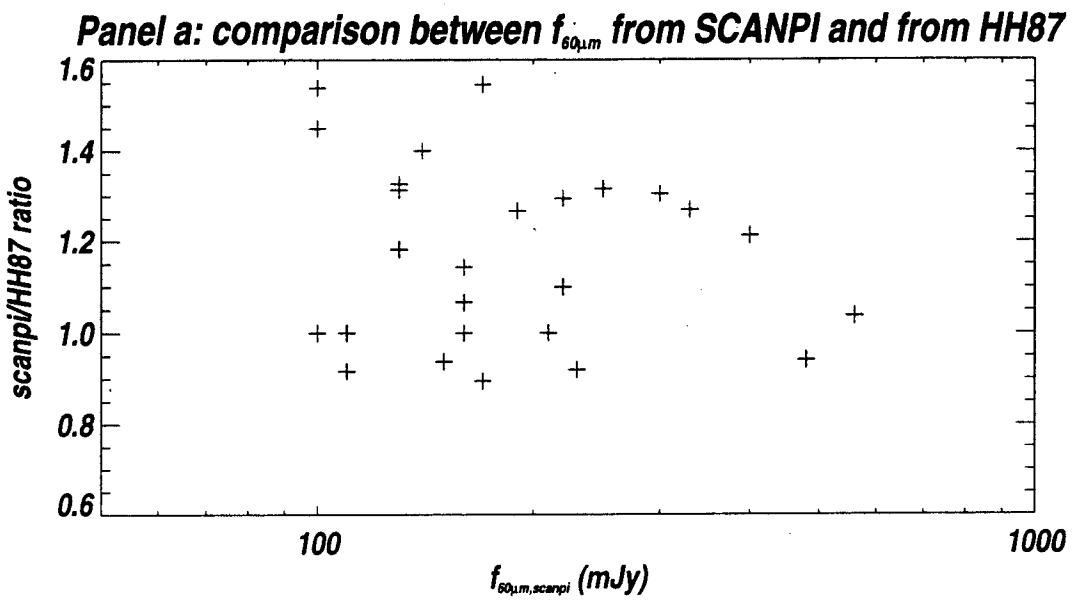
Panel a: comparison between $f_{60\mu m}$ from SCANPI and from HH87
scanpi/HH87 ratio
1.6
1.4
1.2
1.0
0.8
0.6
100
1000
$f_{60\mu m,scanpi}$ (mJy)

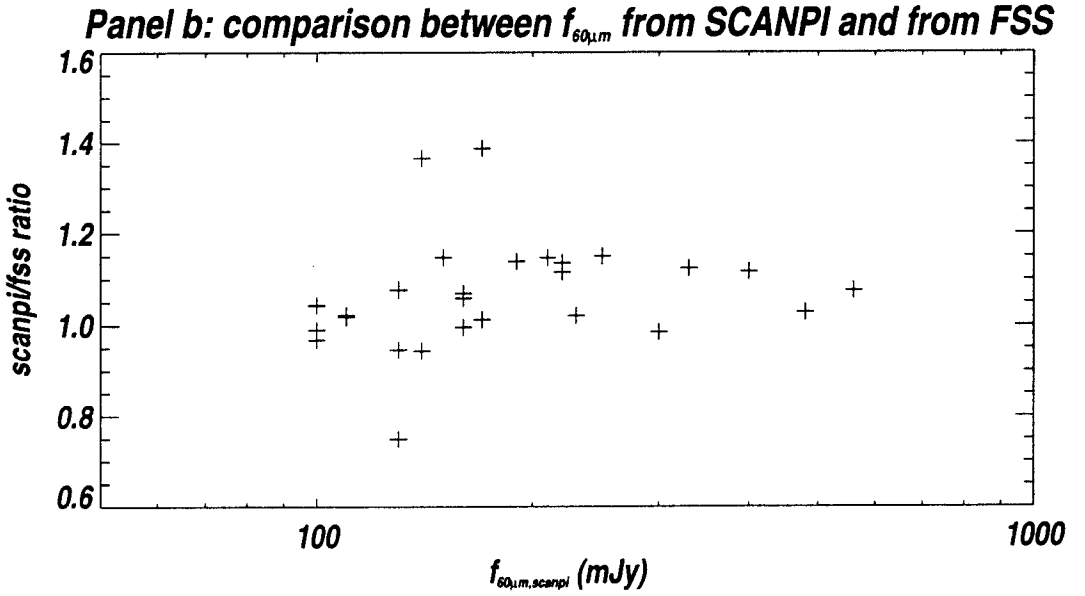
Panel b: comparison between $f_{60\mu m}$ from SCANPI and from FSS
scanpi/fss ratio
1.6
1.4
1.2
1.0
0.8
0.6
100
1000
$f_{60\mu m,scanpi}$ (mJy)

Fig. 1.

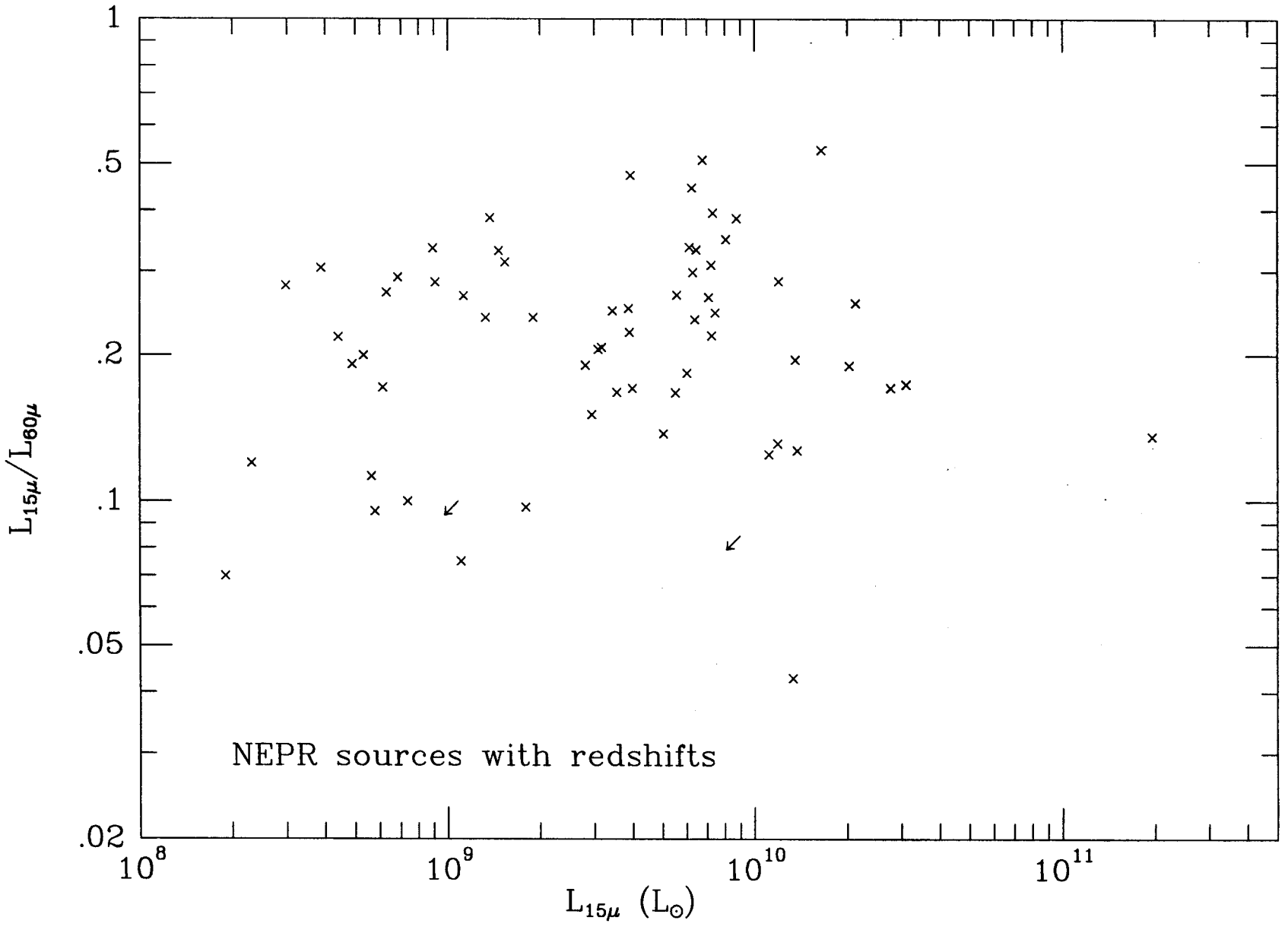
1
.5
.2
.1
.05
.02
$L_{15\mu}/L_{60\mu}$
NEPR sources with redshifts
$10^8$
$10^9$
$10^{10}$
$10^{11}$
$L_{15\mu}$ ($L_\odot$)

Fig 2

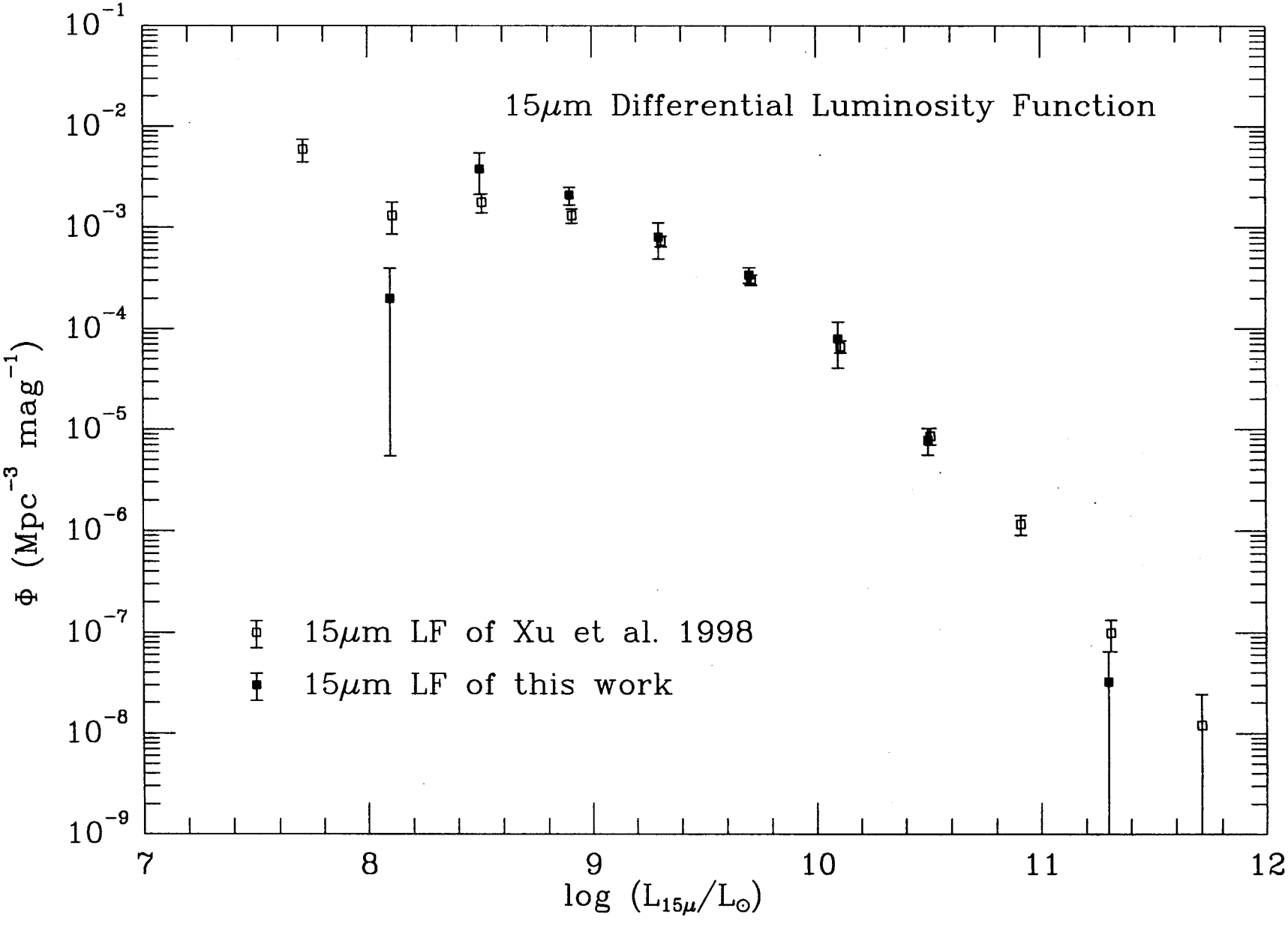
15$\mu$m Differential Luminosity Function
15$\mu$m LF of Xu et al. 1998
15$\mu$m LF of this work
$\Phi$ (Mpc$^{-3}$ mag$^{-1}$)
log ($L_{15\mu}/L_{\odot}$)
$10^{-1}$
$10^{-2}$
$10^{-3}$
$10^{-4}$
$10^{-5}$
$10^{-6}$
$10^{-7}$
$10^{-8}$
$10^{-9}$
7
8
9
10
11
12

Fig 3

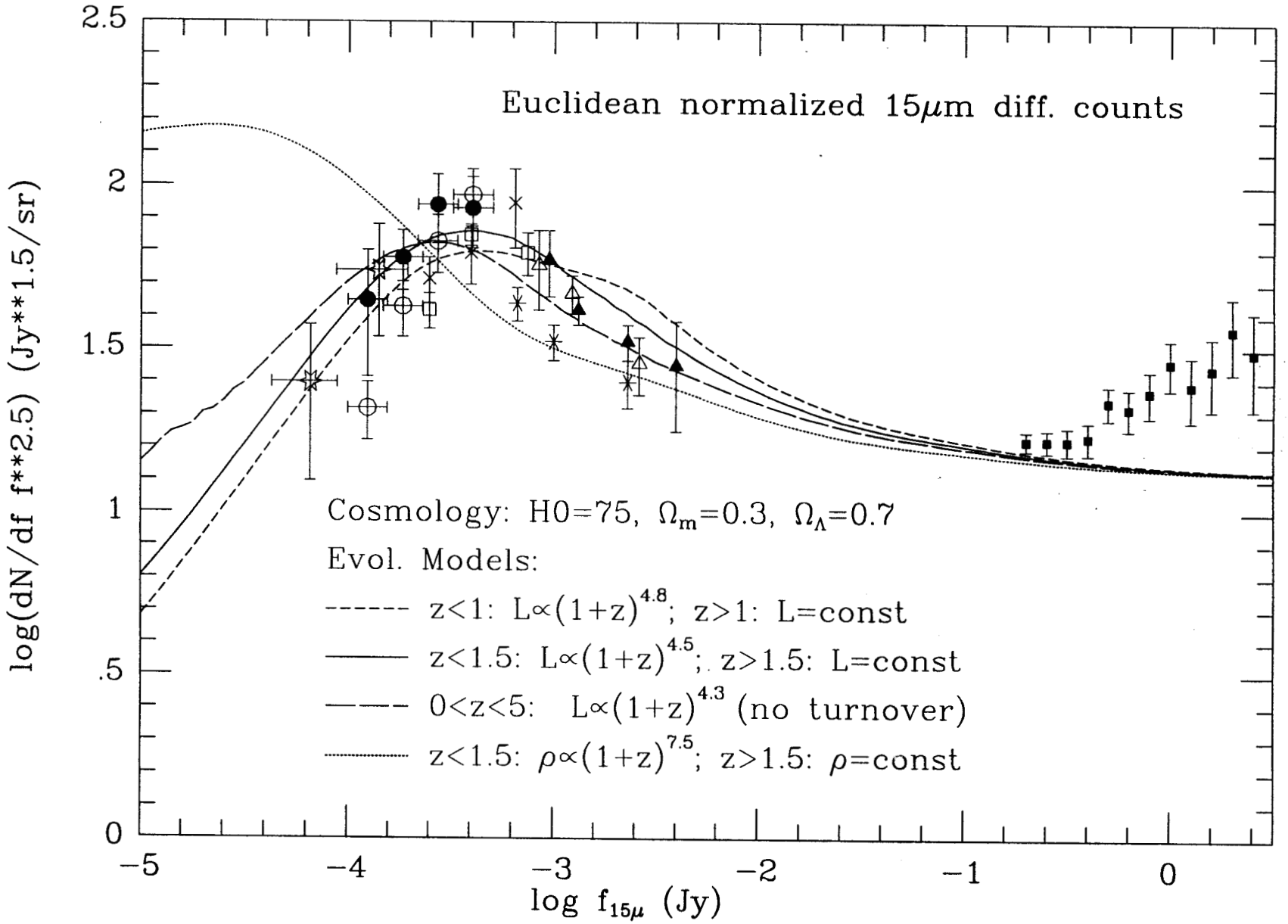
Euclidean normalized 15μm diff. counts
Cosmology: H0=75, $\Omega_m$=0.3, $\Omega_\Lambda$=0.7
Evol. Models:
z<1: L∝(1+z)^4.8; z>1: L=const
z<1.5: L∝(1+z)^4.5; z>1.5: L=const
0<z<5: L∝(1+z)^4.3 (no turnover)
z<1.5: ρ∝(1+z)^7.5; z>1.5: ρ=const
log(dN/df f**2.5) (Jy**1.5/sr)
log f15μ (Jy)
2.5
2
1.5
1
.5
0
−5
−4
−3
−2
−1
0

Fig 4

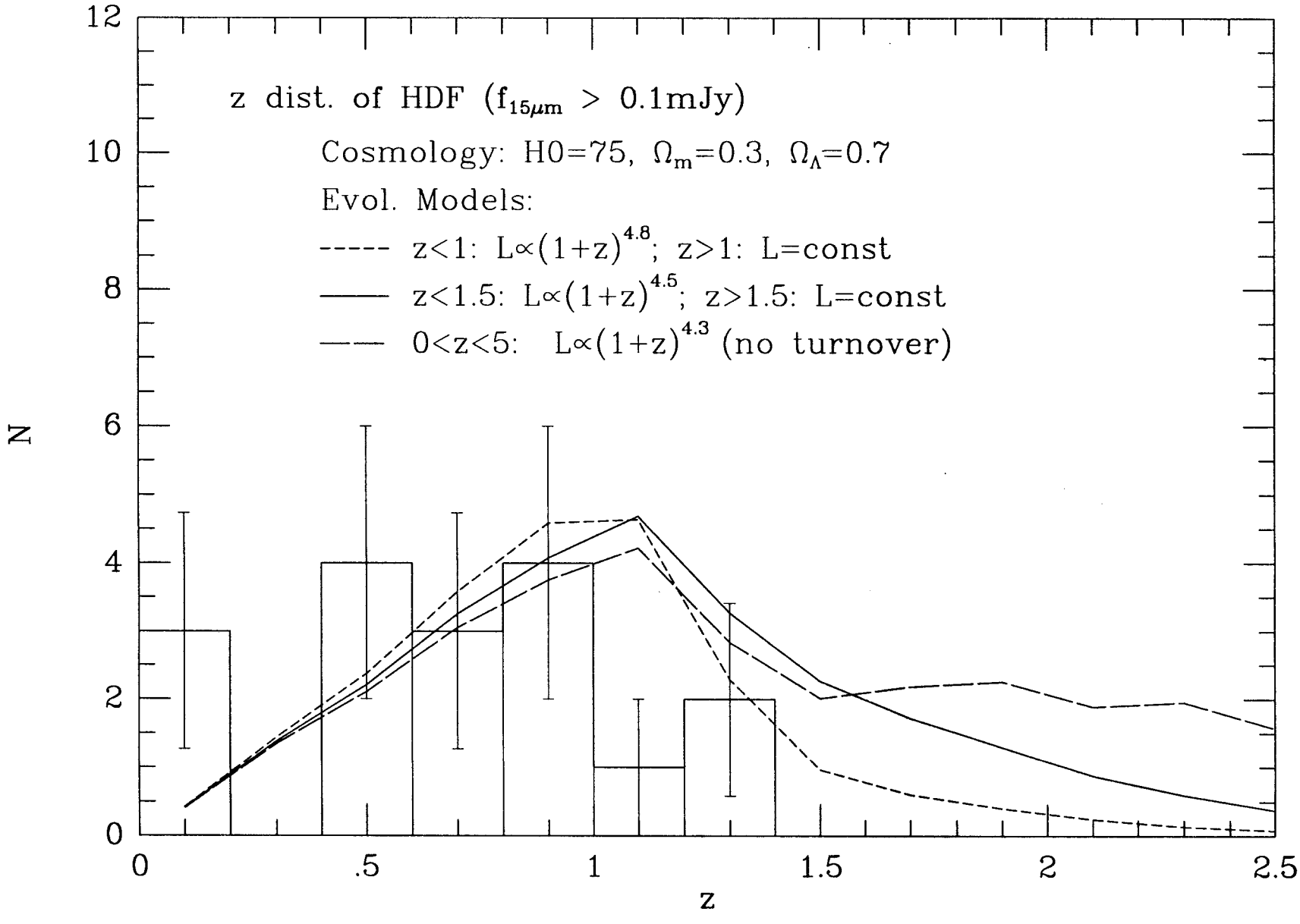
z dist. of HDF ($f_{15\mu m}$ > 0.1mJy)
Cosmology: H0=75, $\Omega_m$=0.3, $\Omega_\Lambda$=0.7
Evol. Models:
----- z<1: L∝(1+z)^4.8; z>1: L=const
—— z<1.5: L∝(1+z)^4.5; z>1.5: L=const
—— 0<z<5: L∝(1+z)^4.3 (no turnover)
N
z
0
.5
1
1.5
2
2.5
0
2
4
6
8
10
12

Fig. 5

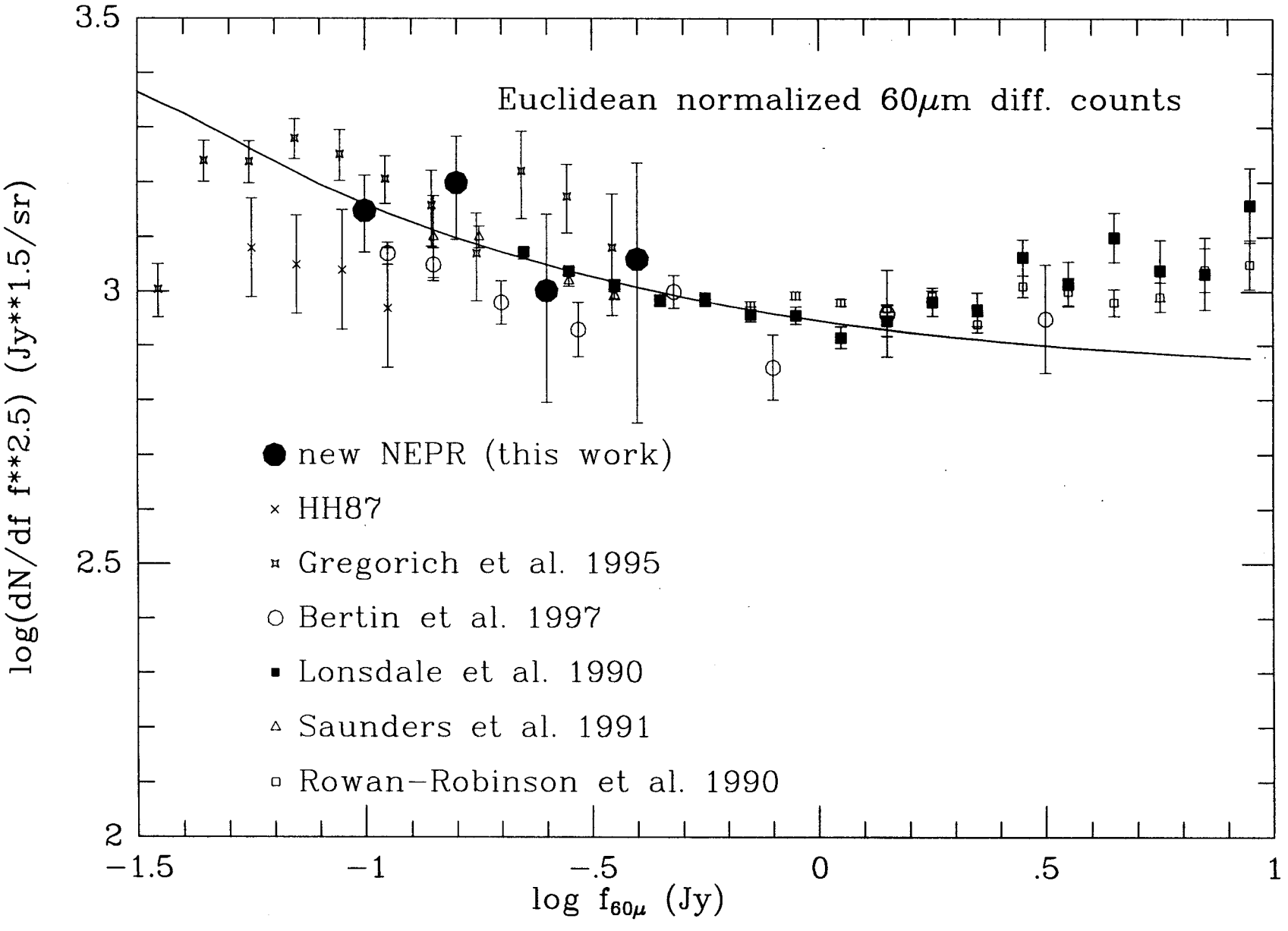
Euclidean normalized 60μm diff. counts
new NEPR (this work)
HH87
Gregorich et al. 1995
Bertin et al. 1997
Lonsdale et al. 1990
Saunders et al. 1991
Rowan-Robinson et al. 1990
log(dN/df f**2.5) (Jy**1.5/sr)
log f60μ (Jy)
3.5
3
2.5
2
−1.5
−1
−.5
0
.5
1

Fig. 6

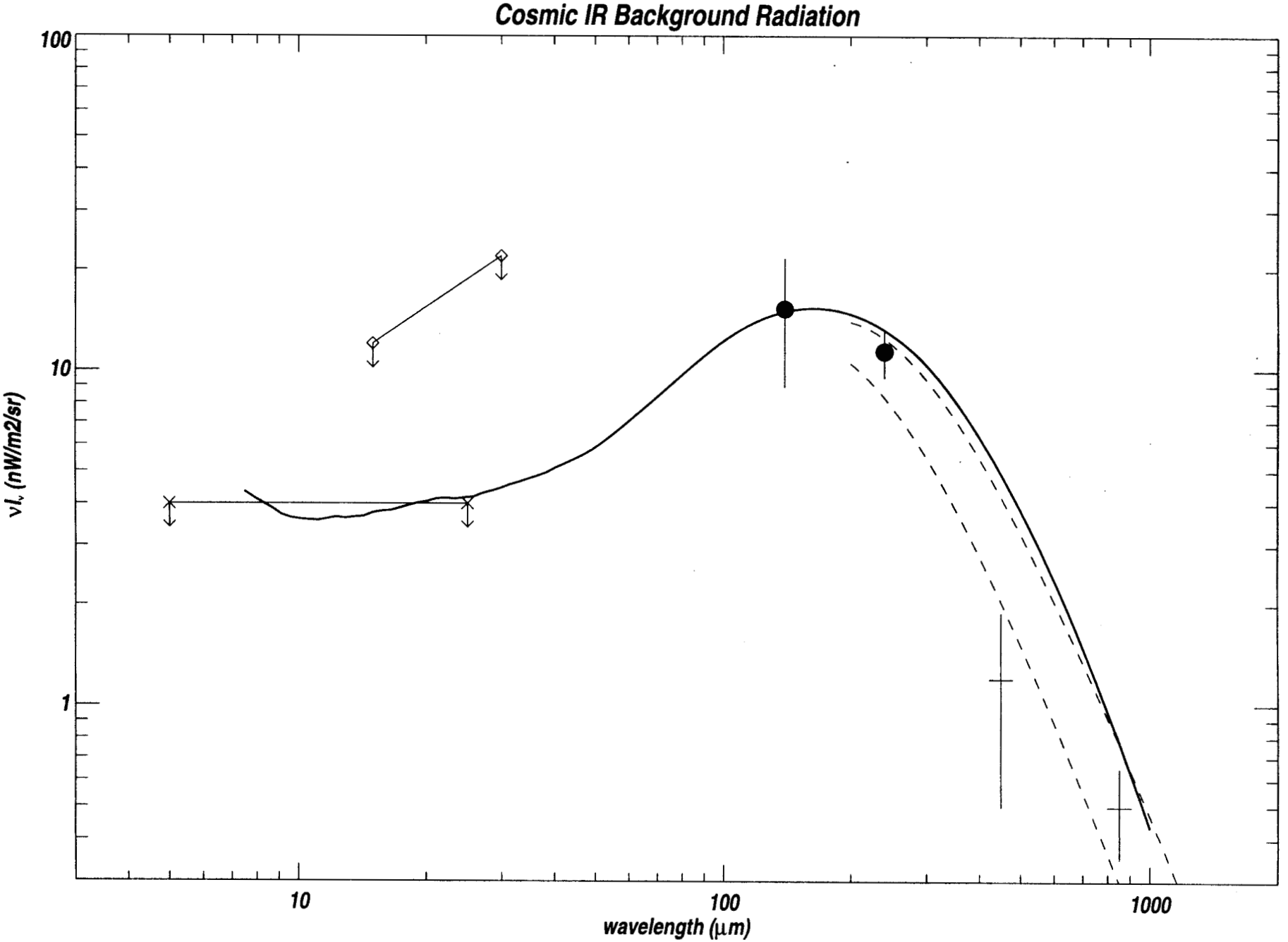
Cosmic IR Background Radiation
100
10
1
νI_ν (nW/m2/sr)
10
100
1000
wavelength (μm)

Fig 2